

Article

# Microstructure and High Temperature Tensile Properties of Mg–10Gd–5Y–0.5Zr Alloy after Thermo-Mechanical Processing

Guohua Wu <sup>†</sup>, H. R. Jafari Nodooshan <sup>†</sup>, Xiaoqin Zeng <sup>\*</sup>, Wencai Liu <sup>\*</sup>, Dejiang Li and Wenjiang Ding

National Engineering Research Center of Light Alloy Net Forming and Key State Laboratory of Metal Matrix Composite, Shanghai Jiao Tong University, Shanghai 200240, China; ghwu@sjtu.edu.cn (G.W.); hamidj\_63@sjtu.edu.cn (H.R.J.N.); lidejiang@sjtu.edu.cn (D.L.); wjding@sjtu.edu.cn (W.D.)

<sup>\*</sup> Correspondence: xqzeng@sjtu.edu.cn (X.Z.); liuwc@sjtu.edu.cn (W.L.); Tel.: +86-21-54742301 (X.Z. & W.L.); Fax: +86-21-34203098 (X.Z. & W.L.)

<sup>†</sup> These authors contributed equally to this work.

Received: 23 October 2018; Accepted: 19 November 2018; Published: 23 November 2018



**Abstract:** The microstructure, high-temperature tensile properties and fracture behavior of the Mg-10Gd-5Y-0.5Zr alloy after thermo-mechanical processing (pre-tension between solution and aging treatment) were investigated. The pre-deformed alloy shows the accelerated aging kinetics compared to the un-deformed alloy. Microstructure of pre-deformed samples showed not only the homogeneous nucleation of the precipitate but also heterogeneous nucleation of precipitates on the dislocation and twin boundaries. Tensile results show that the pre-deformation enhanced the strength of the alloy, while it deteriorates the ductility of the alloy. The ultimate tensile strength (UTS) of the T6 treated un-deformed and pre-deformed alloy at room temperature are 331 MPa and 366 MPa, respectively. Tensile strength of the T6 treated alloy in both un-deformed and deformed conditions was enhanced by raising the test temperature and then reduced by further raising the test temperature. The higher strength of the pre-deformed alloy could be related to the higher density of the precipitates, which grow on the twin boundaries and can hinder the dislocation movement and strengthen the alloy. The results shows that thermo-mechanical processing can significantly improve the room- and high-temperature mechanical properties and enhance the formation of precipitates in Mg-10Gd-5Y-0.5Zr alloy, which can lead to wider application of the alloy in industries such as aerospace or powertrains that need better room- and high-temperature mechanical properties.

**Keywords:** Mg-Gd-Y-Zr alloy; microstructure; thermo-mechanical processing; high temperature mechanical properties

## 1. Introduction

Recently, magnesium alloys have attracted great interest for applications in the automotive and aerospace industries owing to their strong need for lighter vehicles to reduce fuel consumption [1]. Addition of rare earth elements is one of the promising ways to enhance the room- and high-temperature mechanical properties and creep resistance of magnesium alloys [2–9]. Since the solubility of the rear earth elements declines with reducing temperature, the strength of these alloys is essentially enhanced by precipitation strengthening [1,10]. With the purpose of enhancing the mechanical properties of these alloys, many efforts have been made to optimize the precipitation and microstructure by alloying, particularly by rare earth (RE) elements such as gadolinium (Gd), yttrium (Y), samarium (Sm), erbium (Er), and neodymium (Nd) [2–4,8,11]. However, addition of rare earth elements to magnesium alloys can improve the strength of the alloy but is costly

and restricts the applications of the alloys due to deterioration of elongation. Contrary to the variety of research into alloy systems, few studies have been done on the processing approaches to enhance the strength, ductility and age-hardening responses in Mg–RE alloys. Recently Nie et al. reported that annealing the pre-deformed Mg–Gd binary alloy enhanced the strength of the alloy due to the segregation of solute atoms into the twin boundaries [12]. The solute atoms along twin boundaries pinned the twin boundary sliding, thereby strengthening the alloy. Chen et al. [13] studied the effect of annealing on the strengthening of pre-deformed Mg–10Gd–3Y–0.5Zr alloy, and reported that during solution treatment the solute atoms segregated into the deformation twin boundaries and strengthened Mg–10Gd–3Y–0.3Zr alloy; moreover, it was reported that gadolinium solute atoms had a stronger strengthening effect than yttrium atoms. Zhao et al. [14] studied the effect of pre-compression plastic deformation between solution and artificial aging treatment on the microstructure, tensile properties and fracture behavior of the Mg–2.7Nd–0.4Zn–0.5Zr alloy. It was reported that, compared to un-deformed samples, the pre-deformed samples offered a higher volume fraction of precipitates after the aging treatment and had higher strength compared to the un-deformed samples. Induced pre-tension to 10% in Mg–11Gd–2Nd–0.5Zr (wt%) alloy speeds up the aging kinetics and improves the mechanical properties of the alloy [15]. It would seem such thermo-mechanical processing significantly improves precipitation hardening by heterogeneous nucleation on equilibrium state dislocations and enhances the strength of the alloy. Hence it is appropriate to introduce pre-deformation to Mg–RE alloys instead of increasing the content of costly RE elements. However, such thermo-mechanical treatment with pre-tension after solution treatment and prior to artificial aging treatment has been widely reported in Al alloys [16–19], but rarely in Mg alloys. In the present study, pre-tension at room temperature was carried out after solution treatment and prior to aging treatment on Mg–10Gd–5Y–0.5Zr alloy, and the microstructure and high temperature tensile properties of the pre-deformed samples were investigated.

## 2. Experimental Procedures

The ingots of Mg–10Gd–5Y–0.5Zr (all compositions are in wt%) alloy were prepared in an electric resistance furnace from pure Mg (>99.95%), Mg–90Gd, Mg–25Y and Mg–30Zr master alloys. The raw materials were melted at 750 °C under a mixture of CO<sub>2</sub> and SF<sub>6</sub> gas with the ratio of 100:1 (for the present experiment, flow rates of CO<sub>2</sub> and SF<sub>6</sub> are 1 L/min and 10 mL/min, respectively). The melt was cast into a steel mold pre-heated to 200 °C, at pouring temperature of 730 °C. The actual chemical composition of the alloy was Mg–9.68Gd–4.74Y–0.49Zr, determined by an inductively coupled plasma analyzer (Perkin Elmer, Plasma-400), and hereafter simplified as Mg–10Gd–5Y–0.5Zr alloy. The thermomechanical treatment is illustrated in Figure 1. Samples were solution treated at 525 °C for 6 h and then quenched in cold water. The as-quenched samples were subjected to plastic tensile strain of 2%, at room temperature (RT). Then, to develop a precipitation hardening an aging treatment at 225 °C for 16 h was used from the solid solution (aging temperature and time optimized by using un-deformed samples). After thermo-mechanical processing, the microstructure was observed optically with a ZEISS microscope. The 4 vol.% nital solution was used to reveal the grain boundaries. Thin foils for the transmission electron microscopy (TEM, JEOL-2100) observations were prepared by twin jet electro polishing and followed by low energy ion beam milling and carried out at an accelerating voltage of 200 kV. Tensile test was carried out on a Zwick/Roell Z020 tensile testing machine at a temperature range of 25 °C to 300 °C with a speed of 1 mm/min. Rectangular tensile samples with gauge dimension of 2 mm × 3.5 mm × 15 mm were used. For each alloy and temperature, 2 or 3 samples were tested and the average value reported. Fracture surfaces and longitudinal sections near the failure surfaces of the bars were observed by scanning electron microscopy (SEM).

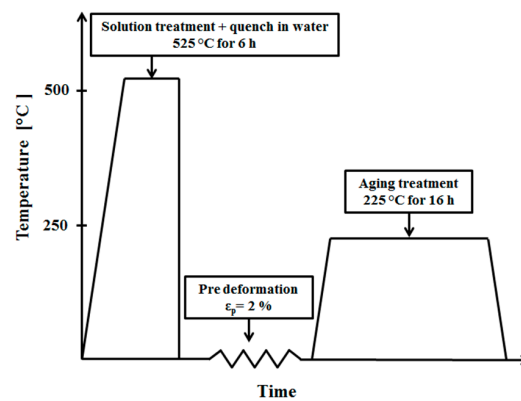


Figure 1. Schematic illustration of thermomechanical treatment process.

### 3. Results

#### 3.1. Microstructure

Figure 2 shows the optical images of as-cast, un-deformed as-quenched and pre-deformed as-quenched samples. As shown in this figure, the microstructures of the as-cast alloys consist of approximately equiaxed dendrites and grains of  $\alpha$ -Mg surrounded by a divorced eutectic of  $\alpha$ -Mg solid solution and rare earth rich intermetallic compounds. After solution treatment, the eutectic network was completely dissolved to the matrix, as is shown in Figure 2b. Figure 2c shows the optical image of the quenched specimen with strain of 2%; the alloy possessed a high density of twins and dislocations which varied for each grain. TEM-BF (TEM bright field) images from the dislocations and twins in the solution-treated samples with 2% strain are shown in Figure 3. The dislocation substructure in the as-deformed samples was recorded by transmission electron microscope under two beam condition with  $g = \{0\ 1\bar{1}1\}_\alpha$  and  $B = 2\bar{1}10_\alpha$ . From Figure 3 it is clear that dislocations lay mostly on basal planes, indicating the basal slip mechanism of deformation in the as-quenched sample. SEM images of the un-deformed and pre-deformed samples after aging at 225 °C for 16 h are illustrated in Figure 4. It can be seen from Figures 2 and 4 that there are no visible changes in the distribution of twins and cuboid-shaped intermetallics after aging treatment.

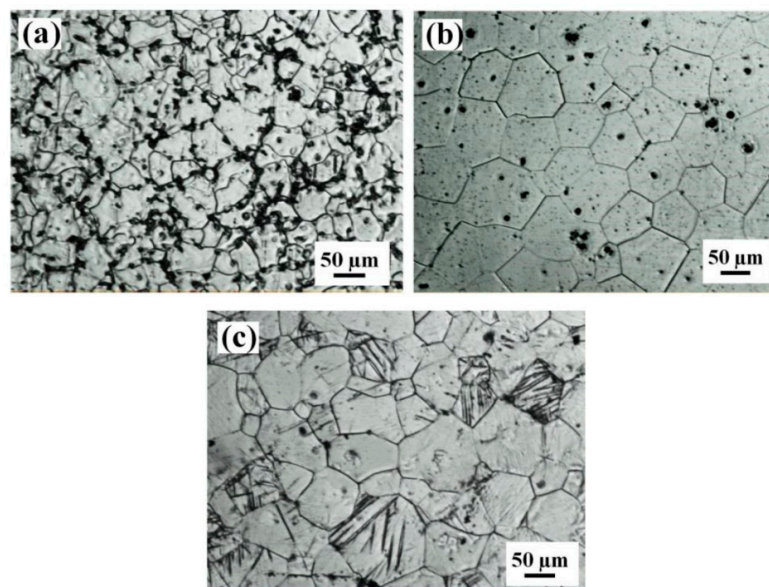
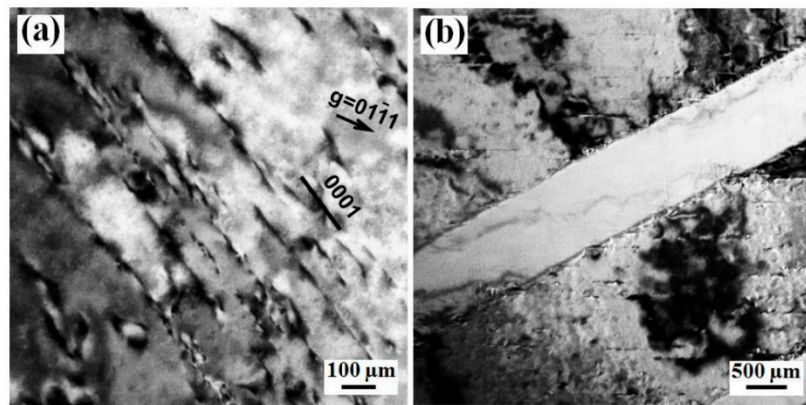
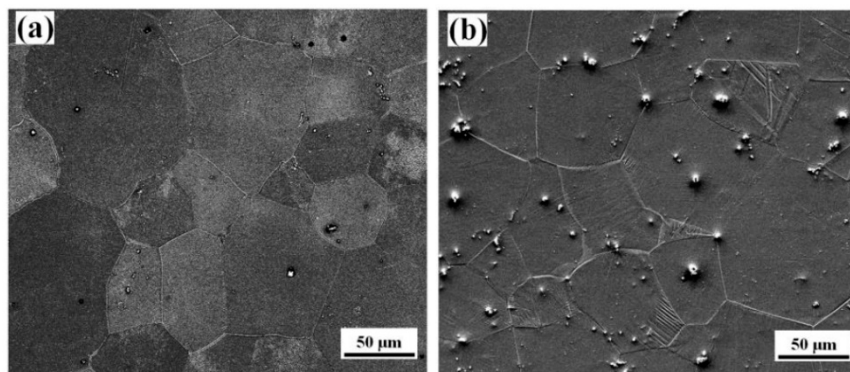


Figure 2. Optical micrograph of (a) as-cast, (b) un-deformed as-quenched and (c) deformed as-quenched Mg–10Gd–5Y–0.5Zr alloy.

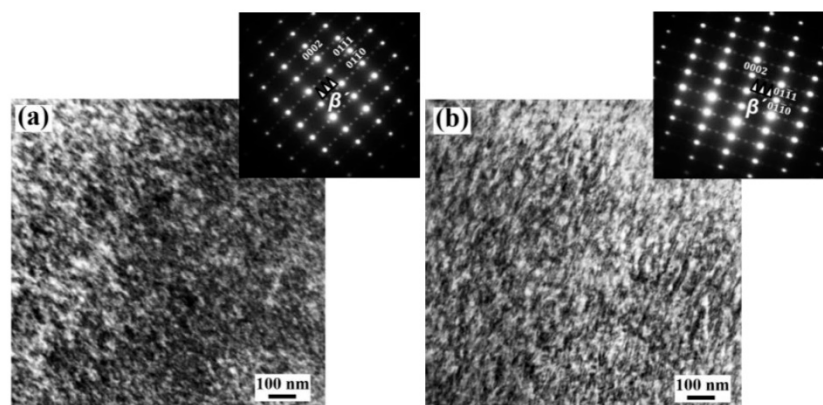


**Figure 3.** Transmission electron microscopy (TEM) bright-field images of the (a) dislocations and (b) twins of deformed as-quenched Mg-10Gd-5Y-0.5Zr alloy.



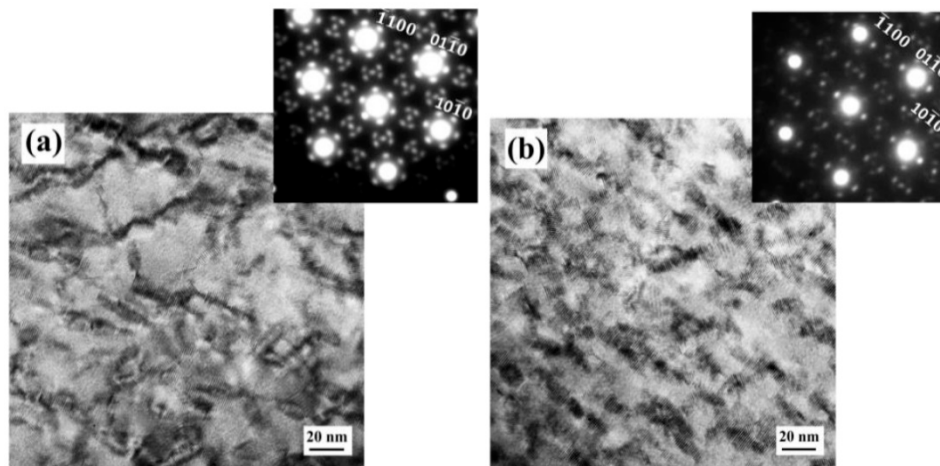
**Figure 4.** Scanning electron microscopy (SEM) images of the (a) un-deformed and (b) pre-deformed Mg-10Gd-5Y-0.5Zr alloy after aging at 225 °C for 16 h.

Figure 5 shows the TEM-BF images of the un-deformed and pre-deformed samples aged at 225 °C for 16 h, with the incident beam approximately parallel to the  $[11\bar{2}0]_{\alpha}$  zone axes. As can be seen from Figure 5, a high density of fine plate-like precipitates presented in the un-deformed and deformed age-treated Mg-10Gd-5Y-0.5Zr alloy. The diffraction spots of equal intensity in  $\frac{1}{4}(01\bar{1}0)_{\alpha}$ ,  $\frac{1}{2}(01\bar{1}0)_{\alpha}$ , and  $\frac{3}{4}(01\bar{1}0)_{\alpha}$  Mg reflections, which is in accordance with the common diffraction pattern of  $\beta'$  precipitate [19,20] are indicated in the inset of Figure 5a,b. The chemical composition of the  $\beta'$  phase was specified by three-dimensional atom probe to be  $Mg_{15}RE_3$  (where RE represents Gd, Y and Zr) and has a base-centered orthorhombic structure (bco,  $a = 0.64$  nm,  $b = 2.22$  nm,  $c = 0.52$  nm) [20].



**Figure 5.** TEM bright field and the corresponding selected area electron diffraction (SAED) pattern of the age-treated (a) un-deformed and (b) pre-deformed Mg-10Gd-5Y-0.5Zr alloy ( $B // [11\bar{2}0]_{\alpha}$ ).

TEM images recorded from un-deformed and pre-deformed specimens after aging treatment, with an incident beam parallel to  $[0001]_{\alpha}$ , are shown in Figure 6. It can be seen from Figure 6 that the volume fraction of the  $\beta'$  precipitate in the pre-deformed specimen is higher than that in the un-deformed sample. SEM and TEM images in Figure 7 show the precipitates that heterogeneously nucleated on the twin and on the twin boundaries in the pre-deformed T6 treated alloy, which is in good agreement with previous findings [14,15].



**Figure 6.** TEM bright field and the corresponding SAED pattern of the T6 treated (a) un-deformed and (b) pre-deformed Mg-10Gd-5Y-0.5Zr alloy ( $B//[0001]_{\alpha}$ ).

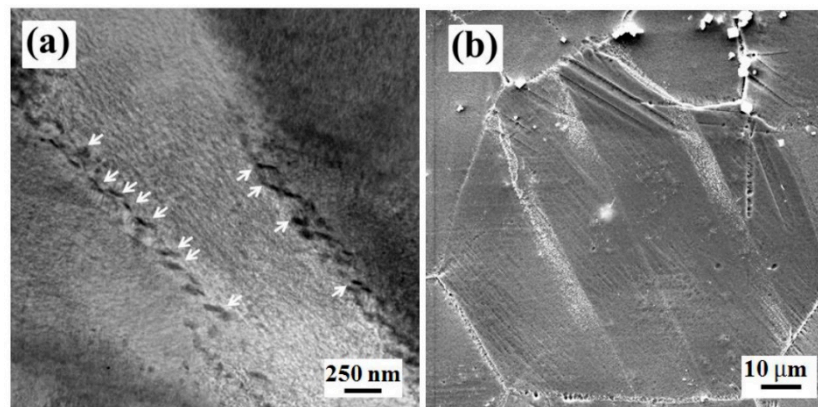


**Figure 7.** TEM and SEM images showing preferential precipitation at twin boundaries and on the twins in pre-deformed specimen after aging treatment.

### 3.2. Tensile Properties

Figure 8 shows the mechanical properties of the tested alloy at different temperatures in the as-quenched condition and after T6 treatment for the un-deformed and pre-deformed specimens. As can be seen from Figure 8, the strength of the un-deformed alloy was significantly enhanced after aging treatment: the ultimate tensile strength (UTS) of the alloy at room temperature (RT) increased almost 30% after aging treatment. The strength of the pre-deformed alloy in all test temperatures was higher than those of the as-quenched and un-deformed T6 treated alloy. The UTS of the pre-deformed sample at room temperature was almost 9% higher than that of age-treated un-deformed alloy. It has also been reported by other researchers that pre-deformation significantly enhanced the strength of the Mg alloys [13–15]. The UTS of the T6 treated pre-deformed alloy decreased first as the test temperature was raised to 150 °C, then increased with further raising of the test temperature to 200 °C, and decreased with further raising of the test temperature beyond 200 °C. However, the UTS of the T6 treated un-deformed alloy slightly declined as the test temperature was raised to 100 °C, but then

increased and peaked as the test temperature reached 150 °C, before declining as the test temperature was raised further. The as-quenched alloy showed the lowest UTS and YS, with its UTS decreasing as the test temperature rose to 175 °C, before increasing to a test temperature of 250 °C.

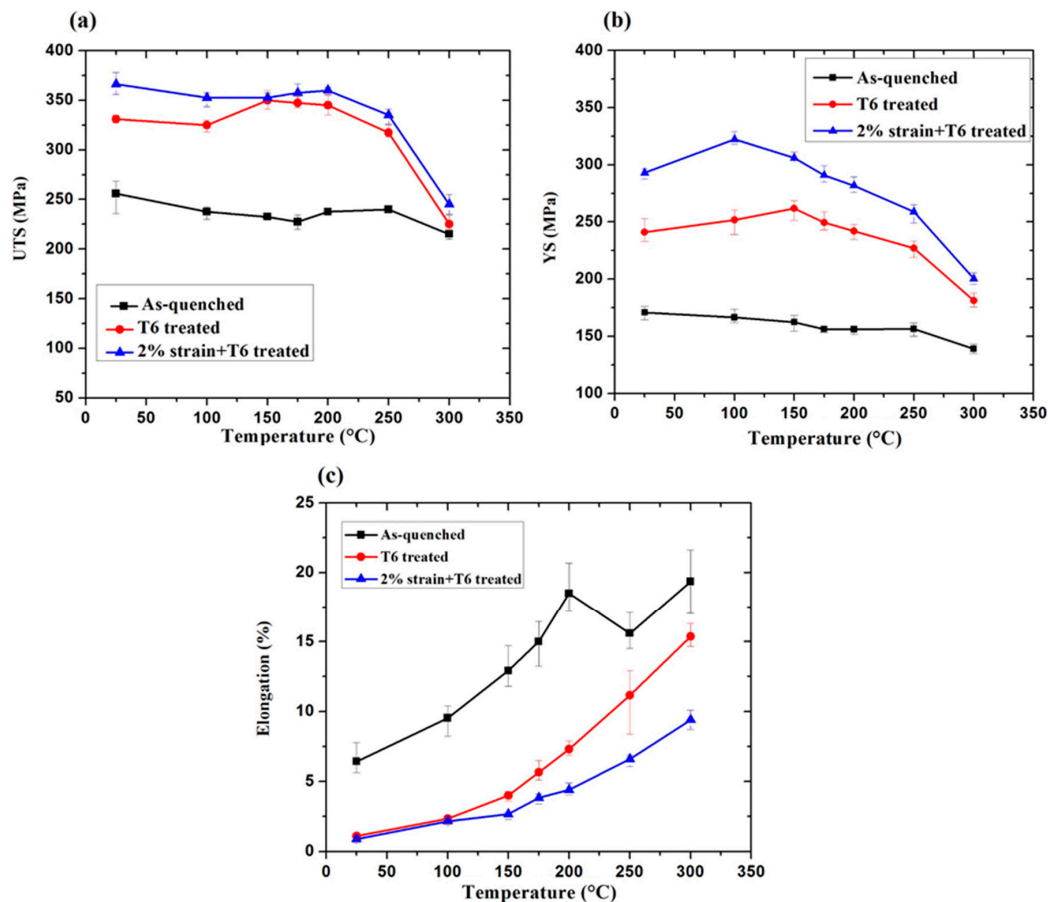


**Figure 8.** (a) Ultimate strength (UTS), (b) yield strength (YS) and (c) elongation of the as-quenched, un-deformed and pre-deformed T6 treated Mg-10Gd-5Y-0.5Zr alloy at temperature range of 25 °C to 300 °C.

Figure 8b shows the yield strength (YS) of the alloy at different conditions versus the test temperature. The pre-deformed alloy showed the maximum value of YS at all temperatures; the YS first increased with rising temperature up to 100 °C and then declined continuously. The un-deformed alloy also showed similar behavior, however, the un-deformed alloy achieved the peak value at 150 °C. The YS of the as-quenched alloy slightly declined with raising the test temperature. The pre-deformation weakens the elongation of the alloy, with the pre-deformed alloy showing the lowest elongation at all of the test temperatures.

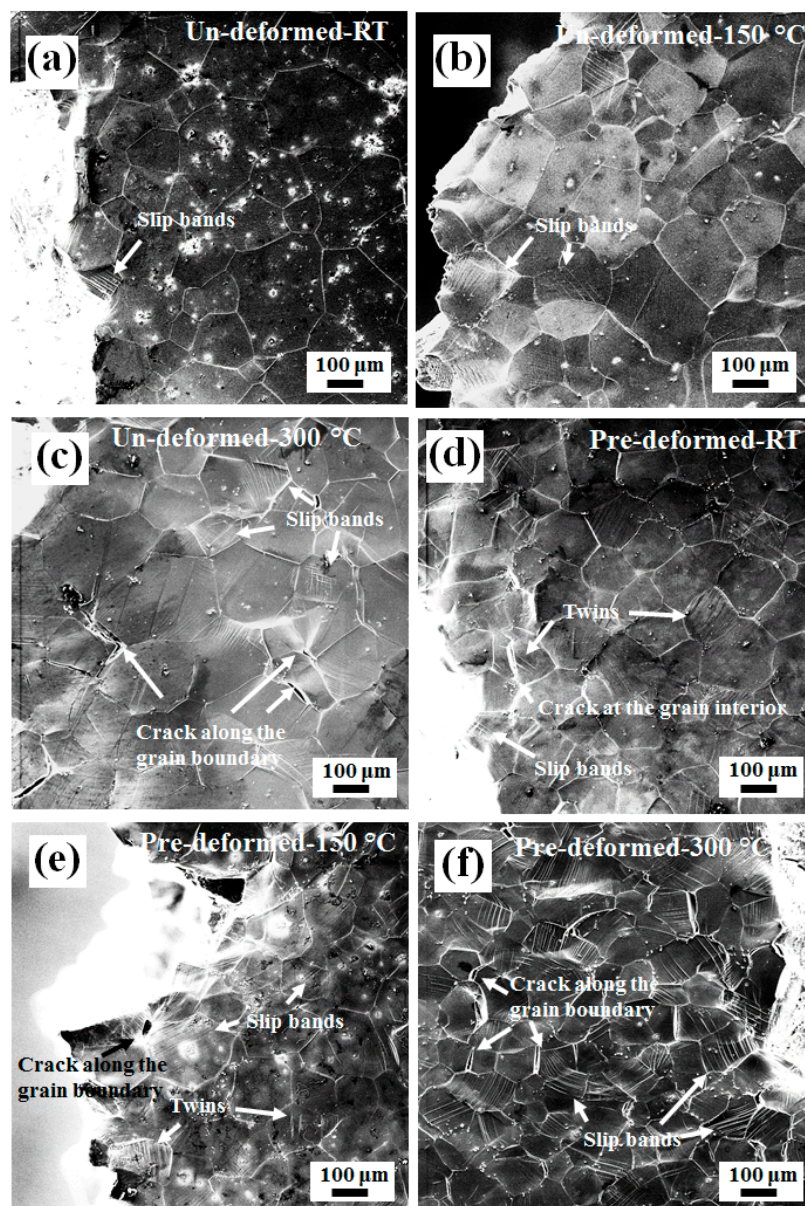
Table 1 compares the values of UTS, YS and elongation of the T6 treated un-deformed and pre-deformed Mg-10Gd-5Y-0.5Zr alloy.

**Table 1.** Tensile properties of the T6 treated un-deformed and pre-deformed Mg-10Gd-5Y-0.5Zr alloy

Condition	Temperature (°C)	UTS (MPa)	YS (MPa)	EL (%)
Un-deformed	25 °C (RT)	331	241	1.1
Un-deformed	150 °C	350	261	4
Un-deformed	300 °C	225	181	15.4
Pre-deformed	25 °C (RT)	366	293	0.9
Pre-deformed	150 °C	352	306	2.6
Pre-deformed	300 °C	245	200	9.4

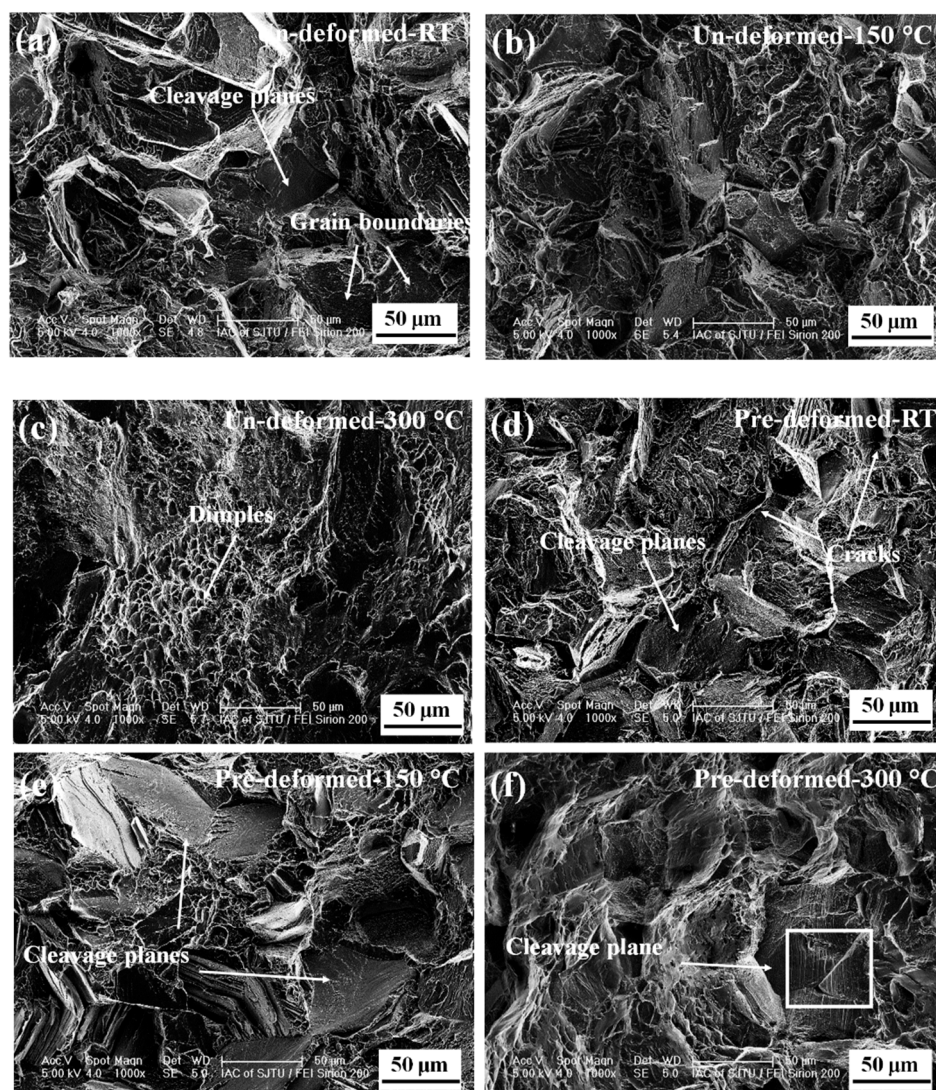
### 3.3. Fracture Behavior

Figure 9 shows the longitudinal section of the fracture surfaces of the un-deformed and pre-deformed Mg–10Gd–5Y–0.5Zr alloy tensile tested at different test temperatures (RT, 150 °C and 250 °C). Evaluation of the microstructure in Figure 9 revealed that pre-deformed and un-deformed alloys at room temperature have a trans-granular fracture, however, the un-deformed alloy after fracture at high temperatures showed a mixture of trans-granular and intergranular fracture mode. As can be seen from Figure 9, microstructure of the pre-deformed alloy at all test temperatures contains a higher number of twins and dislocations. The microstructure of T6-treated pre-deformed alloy after tensile test at 250 °C (Figure 9f) contains many stair-like slip traces in most of the grains exhibiting multiple slip traces. At higher temperature (250 °C) more multiple-slip evidence was observed compared to that of lower temperatures.



**Figure 9.** SEM images of longitudinal section of the fracture surfaces of the T6 treated un-deformed (a–c) and pre-deformed Mg–10Gd–5Y–0.5Zr alloy (d–f) at different temperatures: (a,d) room temperature, (b,e) 150 °C and (c,f) 250 °C.

The fracture features of the T6 treated un-deformed and pre-deformed specimens after tensile testing at different test temperatures are characterized in Figure 10. As can be seen from Figure 10, the fracture surface of the pre-deformed alloy at all test temperatures contains more cleavage planes compared to those of un-deformed specimens. The fracture surface of the pre-deformed sample at room temperature contains cracks and cleavage planes that are characteristic of the brittle fracture. With increasing test temperature, the fracture surface contains less cleavage planes. Figure 10f illustrates the fracture surface of the pre-deformed sample after fracture at 300 °C. The fracture surface of the pre-deformed alloy even after fracture at 300 °C containing cleavage planes, however, the fracture surface of the un-deformed sample after testing at 300 °C mostly contains dimples, which is consistent with higher elongation of the alloy at higher test temperature. The fracture surface of the pre-deformed alloy is in good agreement with low elongation of the alloy at all test temperatures compare to those of the un-deformed samples. It was reported that at higher test temperatures activation of the non-basal slips increases the ductility of magnesium alloys [21].



**Figure 10.** Fractured surfaces of the Mg-10Gd-5Y-0.5Zr alloy un-deformed (a–c) and pre-deformed (d–f) after testing at RT (a,d), 150 °C (b,e) and 300 °C (c,f).

#### 4. Discussion

To further study the effect of precipitation on the high-temperature mechanical properties of the alloy, the Mg-10Gd-5Y-0.5Zr alloy was pre-deformed at the solution stage and then age-treated

at the same temperature and time as the peak age-treated un-deformed Mg-10Gd-5Y-0.5Zr samples. It can be seen from the results that the strength of the alloy at room and high temperatures improved with aging after pre-deformation. The precipitates nucleated on the interior of the twin and twin boundaries in the pre-deformed sample (Figure 7). It has been reported that the aging treatment after pre-deformation causes the nucleation of the precipitates on equilibrium state dislocations as well as twins [18]. TEM images of un-deformed and pre-deformed samples in Figure 6 revealed that the volume fraction of the  $\beta'$  phase in the pre-deformed sample is higher than that in the T6 treated un-deformed sample.

Recently Nie [22] developed appropriate versions of the Orowan equation base on the three main precipitation types in the magnesium alloys. The Orowan gain in critical resolved shear stress (CRSS) needed for dislocations to by-pass the point obstacle is as follows [22–26]:

$$\Delta\tau = \frac{Gb}{2\pi\lambda\sqrt{1-\nu}} \ln \frac{d_p}{r_0} \quad (1)$$

In this formula,  $G$  is the matrix shear modulus ( $G_{Mg} = 1.66 \times 10^4$  MPa [27]),  $b$  is Burgers vector ( $b_{Mg} = 3.21 \times 10^{-10}$  m [27]),  $\lambda$  is the effective planar inter-obstacle spacing,  $\nu$  is Poisson ratio (in magnesium  $\nu = 0.35$  [28]),  $d_p$  is the mean planar diameter of the point obstacles and  $r_0$  the core radius of dislocations.

For prismatic precipitate plates:

$$\lambda = L_p - \frac{d_p}{2} - \frac{\sqrt{3}t_p}{2} = 0.825\sqrt{\frac{d_t t_t}{f}} - 0.393d_t - 0.866t_t \quad (2)$$

$$\Delta\tau = \frac{Gb}{2\pi\sqrt{1-\nu} \left(0.825\sqrt{\frac{d_t t_t}{f}} - 0.393d_t - 0.866t_t\right)} \ln \frac{0.886\sqrt{d_t t_t}}{b} \quad (3)$$

where  $L_p$  is the mean planar center-to-center inter-precipitate spacing,  $d_t$  is the uniform diameter,  $t_t$  is the thickness of precipitate plates, and  $f$  is the volume fraction of precipitates. It has been reported that plate-shaped precipitates that grow on the prismatic plane of the magnesium alloys are the most effective obstacles to the dislocation movement and can enhance the mechanical properties [22]. By increasing the volume fraction and aspect ratio of the precipitates, the strengthening effect will be greater [22]. The improvement of the strength by thermo-mechanical process can be attributed to the higher volume fraction of the  $\beta'$  precipitates in the pre-deformed samples (Figure 6).

As is shown in Figure 8, the T6-treated pre-deformed alloy showed maximum strength at all tensile test temperatures. It is well known that precipitates are the most effective barrier to the dislocation movements and cause enhancement in the strength of the alloy at room and high temperatures. Zhao et al. [14] reported that the higher density of the  $\beta'$  phase in the pre-deformed sample can be the reason for improvement of the strength of the pre-deformed alloy. Nie et al. [12] reported that segregation of Gd atoms into twin boundaries in Mg solid solution minimizes the elastic strains associated with individual Gd atoms, which can cause the decrement of the twin boundary energy and reduce the total energy of the system. The ordered distribution of solute atoms pins the twin boundaries and prevents any further movement of the twin boundary more than individual solute atoms and leads to a larger strengthening effect. Inserting the solute atoms and heterogeneous nucleation of the precipitates on the twinning and dislocations can explain improvement of the strength of the pre-deformed alloy; as was mentioned, the insertion of solute atoms into the twin boundaries or nucleation of the precipitates on the twin boundaries can hinder the migration of the twin boundaries during tensile testing and cause strengthening of the alloy. In addition, the heterogeneous precipitation on the twin boundaries blocked the dislocation crossing the twin boundaries. However, at temperatures higher than 250 °C, the above explanation may not be valid.

It was reported by Barnett et al. [29] that twin presents additional obstacles to dislocation movement. The transformation of dislocations as they pass through the twinning front can establish a high hardening rate in the interior of the twin. As can be seen from Figure 9, the microstructure of the pre-deformed samples after tensile testing at all temperatures contains more twins than that of un-deformed samples at the same temperature. It seems that twin-induced hardening is particularly potent in the pre-deformed samples.

Wang et al. [30,31] reported that multiple slips could strengthen the alloy, since the secondary slip introduces barriers to the primary slip. As can be seen from Figure 9f, the microstructure of the samples after fracture at 250 °C consists of many stair-like lines, which indicate multiple slips. Compared to the un-deformed alloy, the pre-deformed alloy shows a higher number of multiple slips, helping explain the higher strength of the pre-deformed alloy at this test temperature. It is reported that superior high-temperature strength of magnesium alloys containing high amounts of rare earth elements is attributed to the higher density of  $\beta'$  precipitates that grow on the prismatic plane of Mg alloys. These precipitates can prevent the dislocation motion at higher temperatures. The improvement of the strength of the as-quenched alloy at high temperature could be attributed to the dynamic precipitation during high temperature tensile testing.

## 5. Conclusions

The effects of pre-deformation on the microstructure and high temperature tensile properties of an age-treated Mg–10Gd–5Y–0.5Zr alloy were investigated. The obtained results are summarized as follows:

(1) The pre-deformed alloy shows higher density of precipitates compared to the un-deformed sample. Microstructure of deformed samples showed not only the homogeneous nucleation of the precipitate but also heterogeneous nucleation of precipitates on the dislocation and twin boundaries.

(2) Tensile properties of the pre-deformed alloy are higher than those of the un-deformed alloy at all test temperatures. The UTS of the T6-treated pre-deformed alloy at room temperature is 366 MPa, which is almost 9% higher than that of T6-treated un-deformed alloy.

(3) Fracture surfaces of the pre-deformed alloy contain more slip traces and twins compared to that of un-deformed alloy. The fracture surface of the pre-deformed alloy at 250 °C contains many multiple slips. The higher strength of the pre-deformed alloy at higher temperature can be attributed to the multiple slips.

(4) The strength of pre-deformed and un-deformed Mg–10Gd–5Y–0.5Zr alloy was enhanced by raising the test temperature. Improvement of the high temperature strength of the alloy was related to the solution strengthening of rare earth elements and precipitation of  $\beta'$  phases on the prismatic plane.

**Author Contributions:** Supervision, G.W. and W.L.; writing—original draft preparation, H.R.J.N.; investigation, H.R.J.N.; conceptualization, W.L. and H.R.J.N.; writing—review and editing, X.Z., D.L. and W.L.; project administration, W.D.

**Funding:** This work is supported by National Natural Science Foundation of China (Nos. 51775334, 51771115, 51301107, 51474149 and 51601111), National Key Research and Development Program of China (Nos. 2016YFB0301004 and 2016YFB0301002), Science Innovation Foundation of Shanghai Academy of Spaceflight Technology (No. SAST2016048), and Research Program of Joint Research Center of Advanced Spaceflight Technologies (No. USCAST2016-18).

**Conflicts of Interest:** The authors declare no conflict of interest.

## References

1. Honma, T.; Ohkubo, T.; Kamado, S.; Hono, K. Effect of Zn additions on the age-hardening of Mg-2.0Gd-1.2Y-0.2Zr alloys. *Acta Mater.* **2007**, *55*, 4137–4150. [[CrossRef](#)]
2. Wang, J.; Meng, J.; Zhang, D.; Tang, D. Effect of Y for enhanced age hardening response and mechanical properties of Mg-Gd-Y-Zr alloys. *Mater. Sci. Eng.* **2007**, *456*, 78–84. [[CrossRef](#)]

3. Jafari Nodooshan, H.R.; Liu, W.C.; Wu, G.H.; Rao, Y.; Zhou, C.X.; He, S.P.; Ding, W.J.; Mahmudi, R. Effect of Gd content on microstructure and mechanical properties of Mg-Gd-Y-Zr alloys under peak-aged condition. *Mater. Sci. Eng.* **2014**, *615*, 79–86. [[CrossRef](#)]
4. Li, K.J.; Li, Q.A. Microstructure and superior mechanical properties of cast Mg-12Gd-2Y-0.5Sm-0.5Sb-0.5Zr alloy. *Mater. Sci. Eng.* **2011**, *528*, 5453–5457. [[CrossRef](#)]
5. Mahmudi, R.; Kabirian, F.; Nematollahi, Z. Microstructural stability and high-temperature mechanical properties of AZ91 and AZ91+2RE magnesium alloys. *Mater. Des.* **2011**, *32*, 2583–2589. [[CrossRef](#)]
6. Gao, X.; He, S.M.; Zeng, X.Q.; Peng, L.M.; Ding, W.J.; Nie, J.F. Microstructure evolution in a Mg-15Gd-0.5Zr (wt.%) alloy during isothermal aging at 250 °C. *Mater. Sci. Eng.* **2006**, *431*, 322–327. [[CrossRef](#)]
7. Golmakaniyoon, S.; Mahmudi, R. Comparison of the effects of La- and Ce-rich rare earth additions on the microstructure, creep resistance, and high-temperature mechanical properties of Mg-6Zn-3Cu cast alloy. *Mater. Sci. Eng.* **2011**, *528*, 5228–5233. [[CrossRef](#)]
8. Jafari Nodooshan, H.R.; Liu, W.C.; Wu, G.H.; Alizadeh, R.; Mahmudi, R.; Ding, W.J. Microstructure characterization and high-temperature shear strength of the Mg-10Gd-3Y-1.2Zn-0.5Zr alloy in the as-cast and aged conditions. *J. Alloy Compd.* **2015**, *619*, 826–833. [[CrossRef](#)]
9. Jafari Nodooshan, H.R.; Wu, G.H.; Liu, W.C.; Wei, G.L.; Li, Y.L.; Zhang, S. Effect of Gd content on high temperature mechanical properties of Mg-Gd-Y-Zr alloy. *Mater. Sci. Eng.* **2016**, *651*, 840–847. [[CrossRef](#)]
10. Yang, Z.; Li, J.P.; Guo, Y.C.; Liu, T.; Xia, F.; Zeng, Z.W.; Liang, M.X. Precipitation process and effect on mechanical properties of Mg-9Gd-3Y-0.6Zn-0.5Zr alloy. *Mater. Sci. Eng.* **2007**, *454–455*, 274–280. [[CrossRef](#)]
11. Li, Y.L.; Wu, G.H.; Chen, A.; Jafari Nodooshan, H.R.; Liu, W.C.; Wang, Y.X. Effects of Gd and Zr additions on the microstructures and hightemperature mechanical behavior of Mg-Gd-Y-Zr magnesium alloys in the product form of a large structural casting. *J. Mater. Res.* **2015**, *30*, 3461–3473. [[CrossRef](#)]
12. Nie, J.F.; Zhu, Y.M.; Liu, J.Z.; Fang, X.Y. Boundaries periodic segregation of solute atoms in fully coherent twin. *Science* **2013**, *340*, 957–960. [[CrossRef](#)] [[PubMed](#)]
13. Chen, J.; Wang, Z.Q.; Ma, X.G.; Wang, X.H.; Lei, Y.P.; Yan, W. Annealing strengthening of pre-deformed Mg-10Gd-3Y-0.3Zr alloy. *J. Alloy Compd.* **2015**, *642*, 92–97. [[CrossRef](#)]
14. Zhao, S.; Guo, E.; Wang, L.; Wu, T.; Feng, Y. Effect of pre-compressive strain on microstructure and mechanical properties of Mg-2.7Nd-0.4Zn-0.5Zr alloy. *Mater. Sci. Eng.* **2015**, *647*, 28–33. [[CrossRef](#)]
15. Zheng, K.Y.; Dong, J.; Zeng, X.Q.; Ding, W.J. Effect of pre-deformation on aging characteristics and mechanical properties of a Mg-Gd-Nd-Zr alloy. *Mater. Sci. Eng.* **2008**, *491*, 103–109. [[CrossRef](#)]
16. Adrien, J.; Maire, E.; Estevez, R.; Ehrstrom, J.C.; Warner, T. Influence of the thermomechanical treatment on the microplastic behaviour of a wrought Al-Zn-Mg-Cu alloy. *Acta Mater.* **2004**, *52*, 1653–1661. [[CrossRef](#)]
17. Saito, T.; Muraishi, S.; Marioara, C.D.; Andersen, S.J.; Røyset, J.; Holmestad, R. The effects of low Cu additions and predeformation on the precipitation in a 6060 Al-Mg-Si alloy. *Metall. Mater. Trans.* **2013**, *44*, 4124–4135. [[CrossRef](#)]
18. Ringer, S.P.; Muddle, B.C.; Polmear, I.J. Effects of cold work on precipitation in Al-Cu-Mg-(Ag) and Al-Cu-Li-(Mg-Ag) alloys. *Metall. Trans.* **1995**, *26*, 1659–1667. [[CrossRef](#)]
19. Hamanad, D.; Boucheur, M.; Derafa, A. Effect of plastic deformation on the formation and dissolution of transition phases in Al-12 wt.% Mg alloy. *Mater. Chem. Phys.* **1998**, *57*, 99–110. [[CrossRef](#)]
20. Honma, T.; Ohkubo, T.; Hono, K.; Kamado, S. Chemistry of nanoscale precipitates in Mg-2.1Gd-0.6Y-0.2Zr (at.%) alloy investigated by the atom probe technique. *Mater. Sci. Eng.* **2005**, *359*, 301–306. [[CrossRef](#)]
21. Jäger, A.; Lukáč, P.; Gärtnerová, V.; Bohlen, J.; Kainer, K.U. Tensile properties of hot rolled AZ31 Mg alloy sheets at elevated temperatures. *J. Alloy Compd.* **2004**, *378*, 184–187.
22. Nie, J.F. Effects of precipitate shape and orientation on dispersion strengthening in magnesium alloys. *Scripta Mater.* **2003**, *48*, 1009–1015. [[CrossRef](#)]
23. Kelly, A.; Nicholson, R.B. *Strengthening Methods in Crystals*; Elsevier Publishing Company: London, UK, 1971.
24. Ardell, A.J. Precipitation hardening. *Metall. Trans.* **1985**, *16*, 2131. [[CrossRef](#)]
25. Nembach, E. *Particle Strengthening in Metals and Alloys*; John Wiley & Sons: New York, NY, USA, 1997.
26. Reppich, B. *Materials Science and Technology: A Comprehensive Treatment*; Wiley-VCH: Weinheim, Germany, 1993; p. 311.
27. Mabuchi, M.; Higashi, K. Strengthening mechanisms of Mg-Si alloys. *Acta Mater.* **1996**, *44*, 4611–4618. [[CrossRef](#)]
28. Avedesian, M.M.; Baker, H. *Magnesium and Magnesium Alloys*; ASM International: Metal Park, OH, USA, 1999.

29. Barnett, M.R.; Keshavarz, Z.; Beer, A.G.; Atwell, D. Influence of grain size on the compressive deformation of wrought Mg-3Al-1Zn. *Acta Mater.* **2004**, *52*, 5093–5103. [[CrossRef](#)]
30. Wang, H.; Boehlert, C.J.; Wang, Q.D.; Yin, D.D.; Ding, W.J. In-situ analysis of the tensile deformation modes and anisotropy of extruded Mg-10Gd-3Y-0.5Zr (wt.%) at elevated temperatures. *Int. J. Plasticity* **2016**, *84*, 255–276. [[CrossRef](#)]
31. Wang, H.; Boehlert, C.J.; Wang, Q.D.; Yin, D.D.; Ding, W.J. In-situ analysis of the slip activity during tensile deformation of cast and extruded Mg-10Gd-3Y-0.5Zr (wt.%) at 250 °C. *Mater. Charact.* **2016**, *116*, 8–17. [[CrossRef](#)]



© 2018 by the authors. Licensee MDPI, Basel, Switzerland. This article is an open access article distributed under the terms and conditions of the Creative Commons Attribution (CC BY) license (<http://creativecommons.org/licenses/by/4.0/>).